Temperature-dependent Raman scattering and multiple phase coexistence in relaxor ferroelectric Pb(In12Nb12)O3-Pb(Mg13Nb23)O3-PbTiO3 single crystals

J. J. Zhu, K. Jiang, G. S. Xu, Z. G. Hu, Y. W. Li, Z. Q. Zhu, and J. H. Chu

Citation: Journal of Applied Physics **114**, 153508 (2013); doi: 10.1063/1.4825322
View online: http://dx.doi.org/10.1063/1.4825322
View Table of Contents: http://scitation.aip.org/content/aip/journal/jap/114/15?ver=pdfcov
Published by the AIP Publishing

Temperature-dependent Raman scattering and multiple phase coexistence in relaxor ferroelectric $Pb(In_{1/2}Nb_{1/2})O_3$-$Pb(Mg_{1/3}Nb_{2/3})O_3$-$PbTiO_3$ single crystals

J. J. Zhu (诸佳俊),[1] K. Jiang (姜凯),[1] G. S. Xu (许桂生),[2] Z. G. Hu (胡志高),[1,a)]
Y. W. Li (李亚巍),[1] Z. Q. Zhu (朱自强),[1] and J. H. Chu (褚君浩)[1]
[1]*Key Laboratory of Polar Materials and Devices, Ministry of Education, Department of Electronic Engineering, East China Normal University, Shanghai 200241, China*
[2]*R&D Center of Synthetic Crystals, Shanghai Institute of Ceramics, Chinese Academy of Sciences, Shanghai 201800, China*

(Received 19 August 2013; accepted 1 October 2013; published online 16 October 2013)

We report direct observation for the structural transformations of relaxor ferroelectric Pb$(In_{1/2}Nb_{1/2})O_3$-$Pb(Mg_{1/3}Nb_{2/3})O_3$-$PbTiO_3$ single crystals with the aid of temperature-dependent polarized Raman scattering and X-ray diffraction. The cubic to tetragonal phase transition is observed at 460 K and tetragonal to rhombohedral structural transformation takes place at 390 K, which are consistent with the results determined by dielectric spectroscopy. In addition to two well-known phase transitions above room temperature, anomalous structure deformations involving octahedral rotations and tilting angle of polarization can be found around 200 K. A comparison of experimental results with the Devonshire expansion of the free energy by Vanderbilt *et al.* [Phys. Rev. B **63**, 094108 (2001)] allows us to elucidate the peculiar characteristic as the variation of volume fractions among coexistence of three phases, including a first-order phase transition between the orthorhombic and rhombohedral phases and a second-order phase transition between the monoclinic and orthorhombic ones at low temperature. © *2013 AIP Publishing LLC*. [http://dx.doi.org/10.1063/1.4825322]

I. INTRODUCTION

Relaxor-based single crystal of perovskite solid solution $Pb(In_{1/2}Nb_{1/2})O_3$-$Pb(Mg_{1/3}Nb_{2/3})O_3$-$PbTiO_3$ (PIN-PMN-PT) has received much attention because it possesses a relatively higher dielectric permittivities than that of conventional Pb$(Zr_{1-x}Ti_x)O_3$ (PZT) and expanding temperature application range than that of $(1-x)Pb(Mg_{1/3}Nb_{2/3})O_3 - xPbTiO_3$ (PMN-PT).[1,2] There is a great interest for these perovskite solid solutions, especially for morphotropic phase boundary (MPB), in which an intermediate phase or coexistence of multiple phases was found.[3–5] As a key feature of ferroelectric (FE) materials, crystal symmetry is driven by composition as well as temperature. Moreover, its behavior is particularly important in understanding the fundamental properties, such as the FE domain type, spontaneous polarization, dielectric, and optoelectronic response.[5,6]

One of the controversial issues is the structure for the PIN-PMN-PT crystal near the MPB region and its low-temperature evolution is still unresolved. The PIN-PMN-PT crystal is of the cubic structure at high temperature and undergoes a sequence of phase transitions to distorted ferroelectric structures with decreasing the temperature. The structure of the PIN-PMN-PT crystal near the MPB region changes from cubic (C, space group $Pm\bar{3}m$) to tetragonal (T, space group $P4\,mm$) phase at Curie temperature (T_C), tetragonal to rhombohedral (R, space group $R3\,m$) phase at the particular point of T_{R-T}.[7,8] The detailed investigations of PIN-PMN-PT/PMN-PT solid solutions in the MPB region have revealed the presence of an orthorhombic (O, space group $Amm2$) or monoclinic (M_C, space group Pm) bridging phase, which mediates the structural transition from rhombohedral to tetragonal phase.[9–12] Moreover, the orthorhombic/monoclinic symmetry can coexist with a secondary minority rhombohedral or tetragonal phase.[9] Coexistent phases of PIN-PMN-PT system at the MPB region are generally regarded as R + M_C or R + O, since the O phase is the limiting case of the M_C phase when the lattice parameters $a_m = c_m$.[10] That is to say, the M_C phase is a slightly distorted orthorhombic phase. Therefore, many authors consider the M_C phase as a quasiorthorhombic phase and the intermediate phase in the MPB region as M_C/O phase.[9,10] Rhombohedral, tetragonal, orthorhombic, and monoclinic crystal structures are energetically close to each other, which means that the transitions between them are relatively easy by a moderate external field, such as electric and temperature field.[13–15] Although the above concept has been widely accepted for several decades, the critical issue is to answer the following problems: (1) Can the M_C and O phases be distinguished for the perovskite-type relaxor ferroelectrics? (2) What is the underlaying mechanism for the phase coexistence in the PIN-PMN-PT system? (3) What is the main difference on the phase transitions between PMN-PT binary and PIN-PMN-PT ternary oxides?

Following the above considerations, we reported temperature-dependent spectral transmittance of PIN-PMN-PT single crystals with different PT compositions recently.[16,17] It

a)Author to whom correspondence should be addressed. Electronic mail: zghu@ee.ecnu.edu.cn. Tel.: +86-21-54345150. Fax: +86-21-54345119.

was found that the ternary material has positive and negative band gap narrowing trend below room temperature, especially for the MPB region. Based on the band-to-band transitions, the phase transitions can be recognized with the temperature and PT composition. Interestingly, the ferroelectric-paraelectric and ferroelectric-ferroelectric phase transitions above room temperature are consistent with previous reports.[7,8] Therefore, one can expect that the electronic band structure should be directly connected to the crystal structure. In order to further clarify the abnormal variations of electronic transition, the detailed structure study with the temperature is desired for the ternary ferroelectrics.

In the work, a Raman study of the phase transitions on 27PIN-40PMN-33PT and 28PIN-41PMN-31PT single crystals, which are located in the PT-poor region of the MPB with contrary band gap narrowing trends below room temperature, has been presented. In particular, obviously anomalous structures are found below room temperature, which could not be simply interpreted by the R + M_C, where a phase transition cannot occur directly, or R + O, where it is a first-order phase transition according to the eighth-order Devonshire theory.[18] It can be concluded that the anomalous pattern is due to a first-order phase transition between the orthorhombic and rhombohedral phases and a second-order phase transition between the monoclinic and orthorhombic ones at low temperature, with the coexistence of three phases. The present study improves the knowledge of thermal stability for the intermediate phases in the MPB region.

II. EXPERIMENTAL DETAILS

A. Growths of single crystal

The 27PIN-40PMN-33PT and 28PIN-41PMN-31PT single crystals were prepared using a vertical Bridgman technique.[7] The oxide powders with purities better than 99.99%, comprising PbO, In_2O_3, MgO, Nb_2O_5, and TiO_2, were used as starting reagents and mixed according to the formula of 0.27PIN-0.40PMN-0.33PT and 0.28PIN-0.41PMN-0.31PT, respectively. The materials were presynthesized using the two-step Columbite precursor route before being filled into platinum crucibles. PIN-PMN-PT crystals were used as crystal seeds with the diameter size smaller than or equal to the crystal boules. Then, the Pt crucibles were put into alumina crucibles with a supporting setup. The crucible system was driven down through the heat zone at about 1400 °C at a speed of 0.2–0.8 mm/h after socking for more than 10 h. The sample was cut perpendicular to the ⟨001⟩ direction. All PIN-PMN-PT crystals were double-side polished with a mechanical polishing process to smooth the surface. This process consists of three procedures: coarse grinding, fine grinding, and polishing. Then, the crystals were rigorously cleaned in pure ethanol with an ultrasonic bath and rinsed several times by deionized water for spectral measurements.

B. Raman scattering and X-ray diffraction (XRD) measurements

Raman spectra were carried out by a Jobin-Yvon LabRAM HR 800 UV spectrometer with a 488 nm line of an Ar^+ laser as the exciting source. Polarized spectra ⟨x|zz|y⟩ (VV), ⟨x|zx|y⟩ (VH) and depolarized scattering data were recorded from 80 to 800 K by using a Linkam THMSE 600 heating/cooling stage. The laser beam was focused through a 50× microscope with a working distance of 18 mm. An air-cooled charge coupled device (CCD) (−70 °C) with a 1024 × 256 pixels front illuminated chip was used to collect the scattered signal dispersed on 1800 grooves/mm grating.[19,20] The crystalline structure was analyzed by XRD using Ni-filtered Cu Kα radiation (Bruker D8 Advance diffractometer, Germany) under the accelerating voltage of 40 kV at a scanning rate of 3° at 2θ/min. The 2θ range is varied from 15° to 55° at a step of 0.02°. The temperature is varied from 193 to 450 K with a stability of about 0.5 K. Note that no mathematical smoothing has been performed for the experimental Raman and XRD data.

III. RESULTS AND DISCUSSION

A. Polarized and depolarized Raman spectra

Raman spectra of 27PIN-40PMN-33PT and 28PIN-41PMN-31PT crystals at various temperatures are shown in Figs. 1 and 2, respectively. Some main phonon modes can be observed in polarized and depolarized scattering data for two PT compositions. With increasing the temperature, the vibration frequency generally presents a redshift trend. In addition, the two crystals should be located in the MPB region from the electrical measurement.[7] Due to the similarity from two PT compositions, the corresponding discussions, which are based on the PIN-PMN-33PT crystal, can be carried out in the following. The spectra are separated into four characteristic temperature ranges. The change of relative Raman intensities, originating from the cubic to tetragonal phase transition at 460 K, tetragonal to rhombohedral phase transition at 390 K and rhombohedral to coexistence of multiple phases transition at 325 K, and anomalous structure of multiple phases below 300 K, can be seen from Figs. 1(a)–1(c), respectively. Fig. 1(a) shows that the 790 and 600 cm^{-1} modes attenuate obviously from 450 K to 455 K and finally disappear at 460 K, while the 510 cm^{-1} mode becomes more dominant, indicating a ferroelectric-paraelectric phase transition. At the same time, the notable redshift of the 600 cm^{-1} mode in the VV geometry is observed with increasing the temperature, as shown in Figs. 1(d)–1(f). Similar phenomenon is also seen in Raman spectra without polarization from Figs. 1 and 2(g)–2(i). A tiny structure around 280 cm^{-1} is observed above 390 K, which indicates the enhancement of local ordering, marked as an asterisk in Figs. 1 and 2(d), 2(e), 2(g), and 2(h). The 280 cm^{-1} mode is sensitive to the microstructural effects due to the deformation of the angles between oxygen atoms and cations. Other ferroelectric-ferroelectric phase transitions are observed by obvious variations of these phonon modes. It should be emphasized that the distortion of the oxygen octahedral plays an important role in the phonon behaviors. The phase transition features are consistent with the reported results of $T_C \sim 465$ K and rhombohedral to tetragonal phase transition temperature $T_{R-T} \sim 392$ K of 28PIN-40PMN-32PT determined by the dielectric spectroscopy.[7] Note that the spectral shape at low and high temperatures is similar. It indicates that the first-

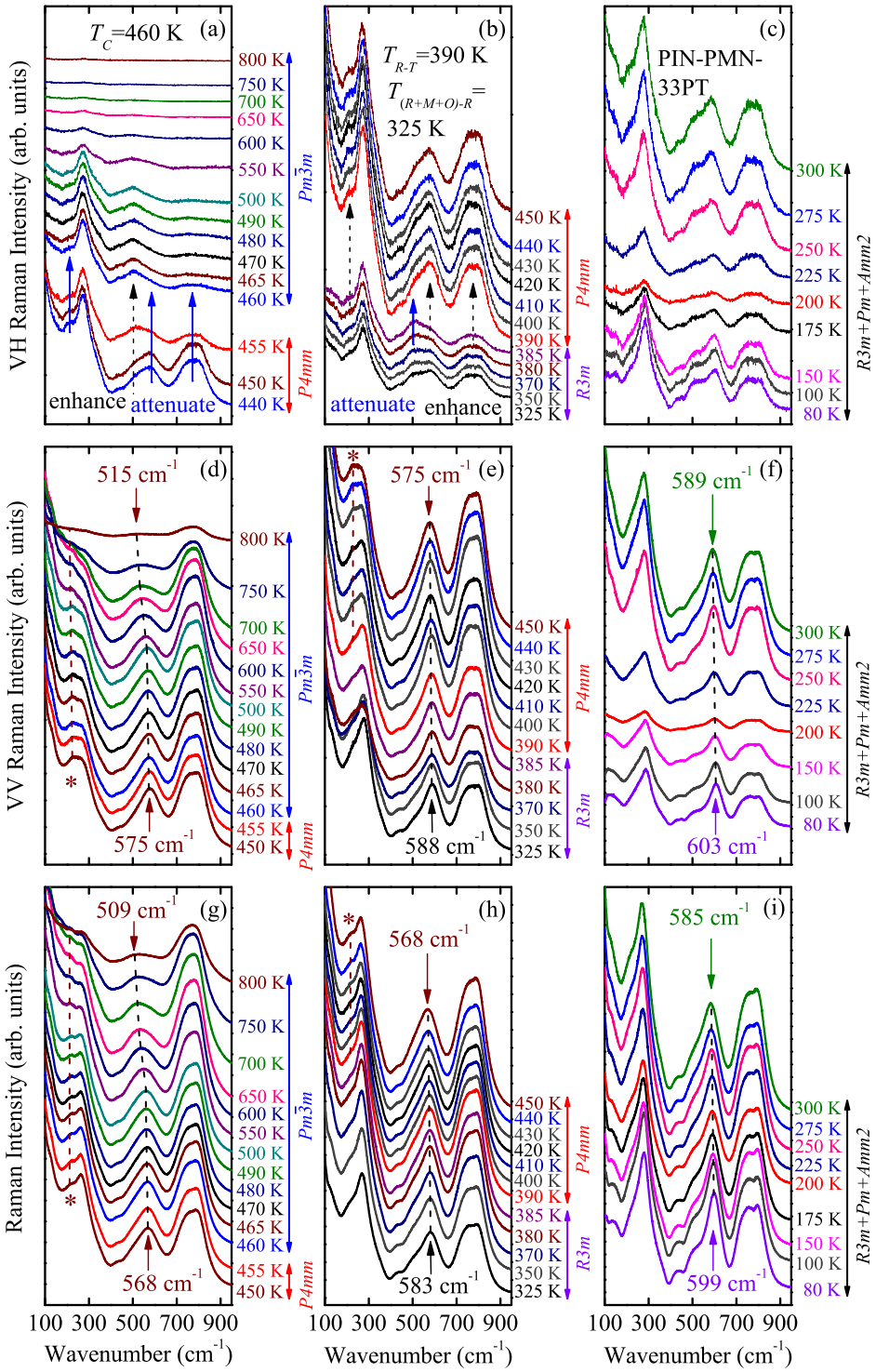

FIG. 1. Raman spectra of the PIN-PMN-33PT crystal (a) around $T_C \sim 460$ K, (b) rhombohedral to tetragonal phase transition temperature $T_{R-T} \sim 390$ K, rhombohedral to the coexistence of multiple phases transition temperature $T_{(R+M+O)-R} \sim 325$ K, and (c) in the multiple coexisting structures below room temperature in ⟨x|zx|y⟩ (VH) scattering geometry, ⟨x|zz|y⟩ (VV) scattering geometry (d)–(f), and depolarized Raman spectra (g)–(i). The wine asterisks together with the wine dotted lines are marks of obvious broadening of the 280 cm^{-1} mode in (d), (e), (g), and (h). Each spectrum is shifted in intensity for clarity.

order Raman scattering is prohibited.[21] The peaks in the spectra of PIN-PMN-PT crystal are induced by local polar structures with different symmetry, which are activated by the broken translational symmetry. Therefore, the sharpness and intensity are connected with the size of the nanopolar clusters and dynamic interactions with the local random fields.

B. Assignment and temperature evolution of phonon modes

Compared with the dimensions of the unit cell in the crystal, the wavelength of phonons in the first-order Raman scattering is infinite.[22,23] However, the phonon modes transform as the irreducible representations of the respective point group at the zone-center Γ of the Brillouin Zone. Only a maximum of $3 \times (r - 1)$ optical modes is probable to be observed at $\mathbf{k} = 0$, where $\mathbf{k}$ is the direction along the crystal axis. The number of atoms in the unit cell r is five for relaxor ferroelectric PIN-PMN-PT with the ABO_3 perovskite structure. In the cubic paraelectric phase ($Pm\bar{3}m$) of PIN-PMN-PT, 12 optical phonon modes transform as the $3T_{1u} + T_{2u}$ irreducible representation. Long-range Coulomb forces lift the degeneracy of the T_{1u} modes into a doubly degenerate T_{1u} (TO) mode and a single T_{1u} (LO) mode, where LO and TO

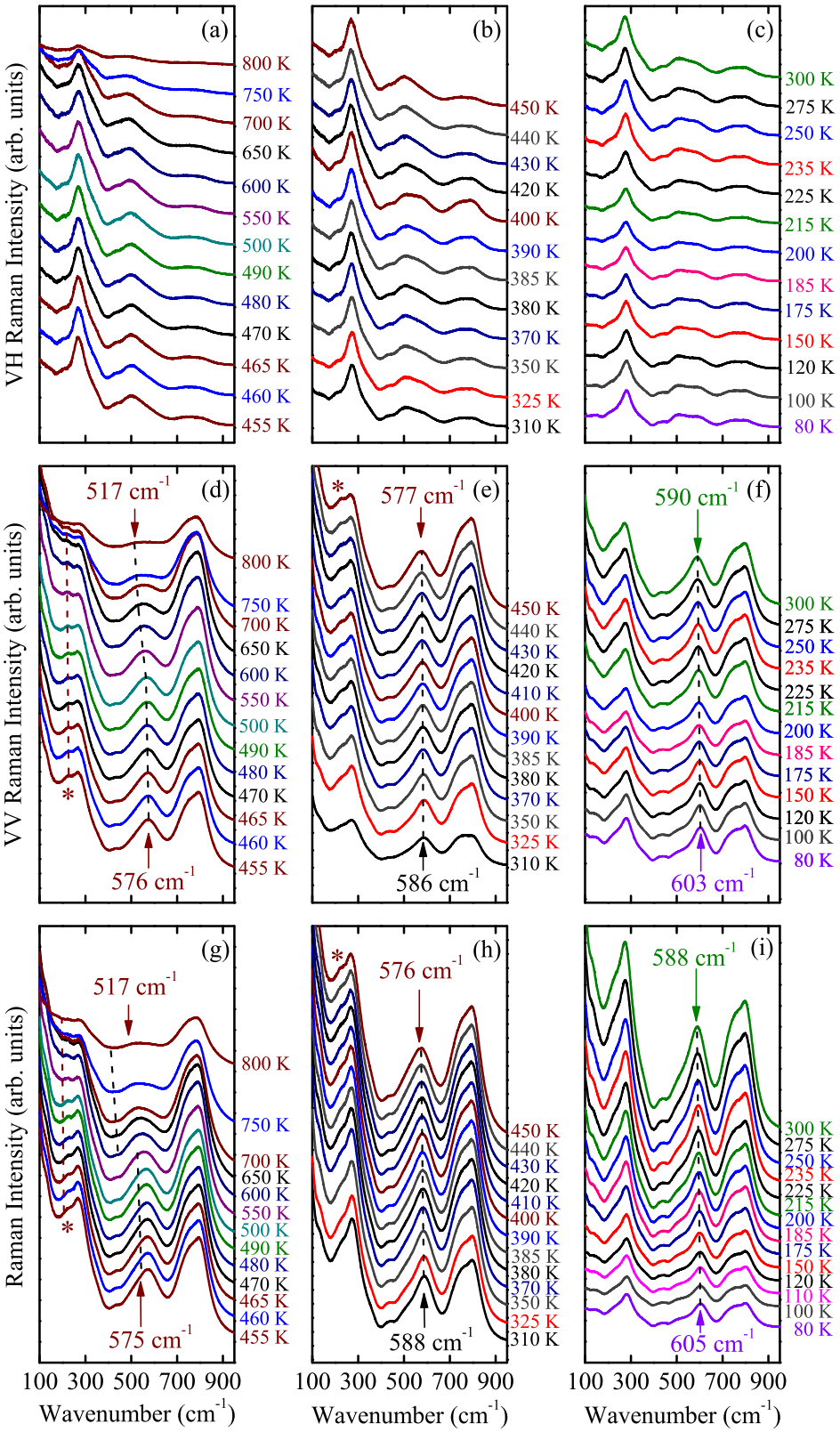

FIG. 2. Raman spectra of the PIN-PMN-31PT crystal (a) around T_C, (b) rhombohedral to tetragonal phase transition temperature T_{R-T}, rhombohedral to the coexistence of multiple phases transition temperature $T_{(R+M+O)-R}$, and (c) in the multiple coexisting structures below room temperature in $\langle x|zx|y\rangle$ (VH) scattering geometry, $\langle x|zz|y\rangle$ (VV) scattering geometry (d)–(f), and depolarized Raman spectra (g)–(i). The asterisks together with the dotted lines are marks of obvious broadening of the 280 cm^{-1} mode in (d), (e), (g), and (h). Each spectrum is shifted in intensity for clarity.

refer to longitudinal and transverse modes, respectively. Upon cooling, the ferroelectric-paraelectric phase transition occurs at 460 K, inducing each $3T_{1u}$ mode splitting as E + A_1 and the nonpolar T_{2u} mode as E + B_1 in the tetragonal phase. The E + B_1 mode is regarded as silent for a long time due to its Coulomb-field splitting and only visible at low temperature.[22,23] The B_1 mode further changes into the A_2 mode below 390 K, where the tetragonal-rhombohedral transition occurs. The A_2 mode of the irreducible representation has no Raman activity in the rhombohedral phase. It transforms into the A′ mode upon transiting to monoclinic phase, while the A_1 mode in the rhombohedral phase transforms into the B_1 mode, with the E mode splitting as the A_1 and B_2 modes in the orthorhombic phase below 300 K.[24] Because

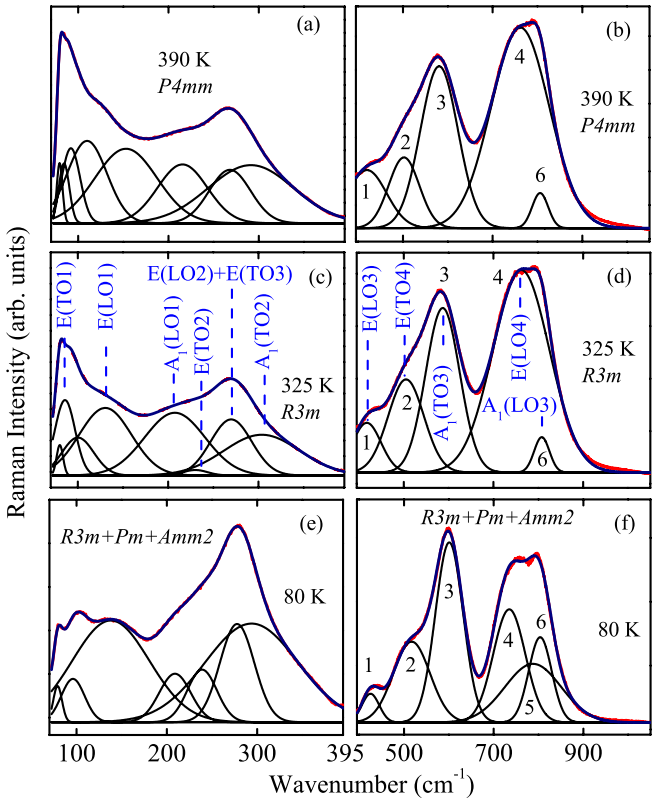

FIG. 3. Deconvolution of the depolarized Raman spectra at 390 K in (a) and (b) tetragonal symmetry, at 325 K in (c) and (d) rhombohedral symmetry, and at 80 K in (e) and (f) coexistence of multiple phase symmetries. The peak positions at 325 K in (c) and (d) are 80, 86, 100, 130, 207, 230, 270, 304, 417, 505, 587, 762, and 808 cm^{-1}. The numbers 1-6 label six Raman modes observed at 80 K in (f). The numeration is kept with increasing the temperature.

the unit cell is unchanged in size upon cooling from the cubic to rhombohedral phase, the critical point of the Brillouin zone of the paraphase is the Γ point. In addition, the Pb ion dynamics play an important role in the change of the Raman spectra with increasing the temperature, which are related to the phase transitions. The symmetry variation deriving from the correlated ion off-center displacements, which grows with decreasing the temperature, can cause the nucleation of regions with different local symmetries.[13]

The deconvolutions of the Raman spectra are presented in Fig. 3 by using a Gauss curve fitting. According to the group theory as well as the results of other relaxors,[21–33] the assignment of phonon modes for PIN-PMN-33PT with the rhombohedral phase is plotted in Fig. 3. For clarity, the comparison for the assignment of modes among PIN-PMN-33PT and other relaxors is listed in Table I. It should be emphasized that there are no reports on the phonon modes of PIN-PMN-PT crystal, even at room temperature. As we can see, most of vibrations can be assigned except for two lower-frequency modes (80 cm^{-1} and 100 cm^{-1}). Generally, it is impossible to expect an excellent compatibility with the theoretical calculation in such disordered material as ternary PIN-PMN-PT system. It is also impossible even for binary PMN-PT system because Raman spectra are very sensitive to the local symmetry.[13] Therefore, it is potential for detecting the presence of the 1:1 order in the B-ion sublattice as well as the coexistence of multiple phases with different lengths of coherence. Monoclinic symmetry can be detected as a long range property at MPB region and in the low temperature. According to the present results, the monoclinic symmetry coexists with other phases, which suggests that it does not exist as a single phase. The frequency, linewidth, and intensity evolution of the selected modes with the temperature are applied to justify the structural changes (Fig. 4).

TABLE I. The phonon mode frequencies of the PIN-PMN-PT single crystals are extracted from the Gauss curve fitting (Figure 3) at 325 K. The experimental and theoretical data from the PMN-40PT crystals have been taken from Ref. 26 and those for $PbTiO_3$ taken from Ref. 27 for comparison. Note that the unit is cm^{-1}.

Phonon modes	PIN-PMN-PT (This work)	PMN-40PT (Exp.)/(Cal.)	$PbTiO_3$
…	80	…	…
E(TO1)	86	91/…	88
…	100	…	…
E(LO1)	130	137/146	128
A_1(LO1)	207	208/187	189
E(TO2)	230	…	220
E(LO2)/E(TO3)	270	265/260	289
A_1(TO2)	304	317/…	359
E(LO3)	417	434/425	439
E(TO4)	505	514/…	505
A_1(LO2)	587	580/589	…
E(LO4)	762	751/714	723
A_1(LO3)	808	797/853	796

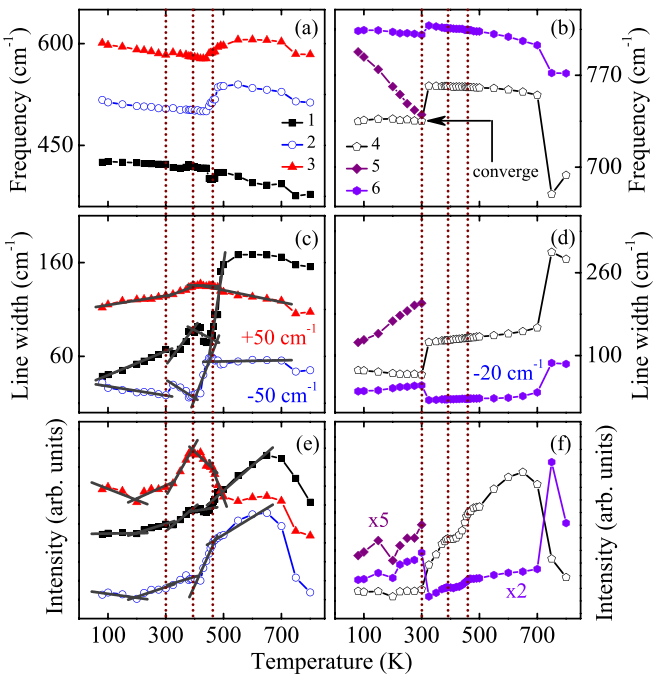

FIG. 4. Evolution of (a), (b) the frequency, (c), (d) the line width, and (e), (f) the intensity of the bands 1-6. Lines are guides for eyes in (c) and (e). The dotted lines show the respective transition temperatures, including T_C at 460 K, rhombohedral to tetragonal phase transition temperature T_{R-T} at 390 K, rhombohedral to the coexistence of multiple phases transition temperature $T_{(R+M+O)-R}$ at 325 K, and the multiple coexisting structures below room temperature. The peak intensity of line 2 in (e) is shifted in intensity for clarity.

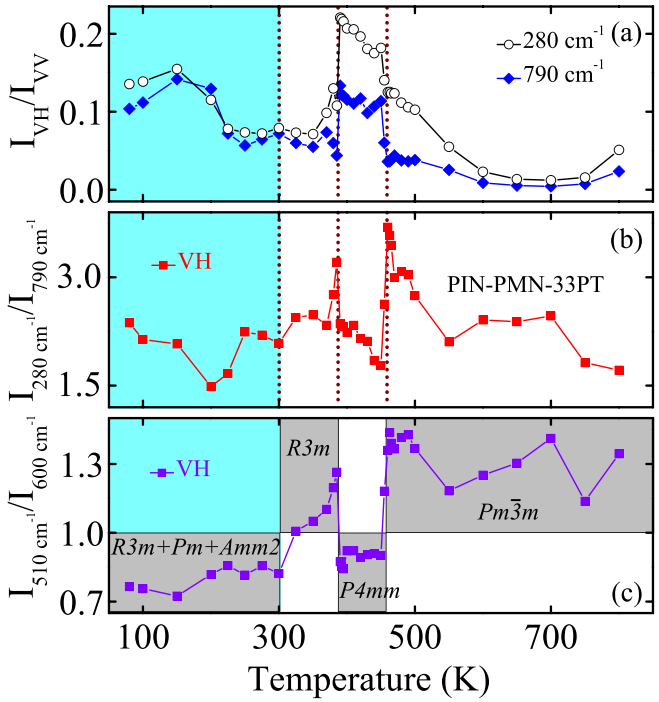

FIG. 5. Temperature dependence of (a) the intensity ratio of the modes at 280 and 790 cm^{-1}, and (b) the intensity ratio between the modes 280 and 790 cm^{-1} in the VH scattering geometry and (c) the intensity ratio between the modes 510 and 600 cm^{-1} in the VH scattering geometry. The dotted lines show the respective transition temperatures, including T_C at 460 K, rhombohedral to tetragonal phase transition temperature T_{R-T} at 390 K, rhombohedral to the coexistence of multiple phase transition temperature $T_{(R+M+O)-R}$ at 325 K, and the multiple coexisting structures below room temperature.

Six obvious phonon modes are observed from 395 to 1150 cm^{-1} below 300 K, while only five ones are distinguished above 325 K, as shown in Figs. 3(b), 3(d), and 3(f). Fig. 4(b) shows that the frequencies of line 4 and line 5 begin to converge upon heating, with the disappearing of line 5 at $T_{(R+M+O)-R} \sim 325$ K. It was reported that there are six corresponding modes for low-temperature phase and five ones

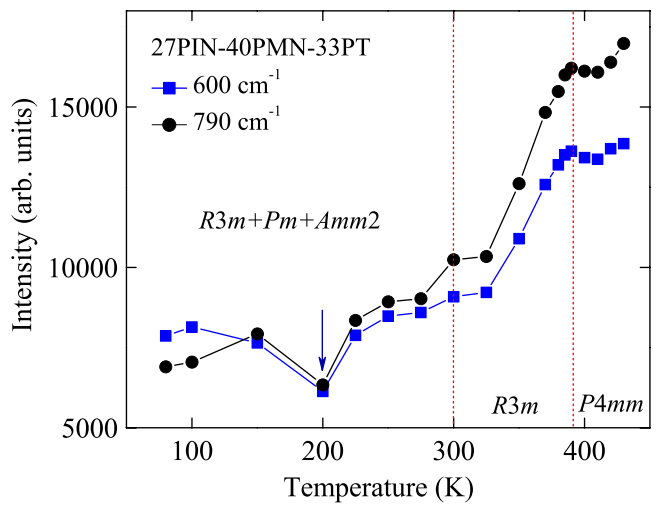

FIG. 6. Temperature dependence of the intensity of the modes at 600 cm^{-1} and 790 cm^{-1} in the depolarized scattering geometry. The dashed lines are the respective transition temperatures. Note that there is a dip at about 200 K.

above room temperature in the case of PMN-PT system near the MPB region.[13] The lattice symmetry of the crystal determines the number of Raman active modes, which is used to detect the phase transformations. However, the present Raman results of the PIN-PMN-PT crystal do not show complete selection rules from the observed modes due to the existence of the polar nanoregions (PNRs) in the relaxor ferroelectrics. The PNRs of the M_C and O symmetries affect the Raman spectra collected within the R one. Therefore, the observed Raman lines come from the coexistence of the R + M_C + O. The intensity and line shapes of Raman spectra in the VV and VH geometry are different due to polarization configurations originating from different tensor. The phase transitions are manifested by the deviations from the linear behavior of line width and intensity in Figs. 4(c) and 4(e), respectively.

C. Phase transitions and low-temperature anomalous structure

The temperature evolution of the intensity ratio $(I_{VH}/I_{VV})_{790\ cm^{-1}}$ indicates structural transformations in the relaxor ferroelectrics,[34] as shown in Fig. 5(a). Obvious decline is observed at T_C, which indicates a ferroelectric-paraelectric phase transition. The difference of Raman tensor components in each phase affects the intensity ratio of these bands. The ratio $I_{280\ cm^{-1}}/I_{790\ cm^{-1}}$ versus temperature in the VH geometry is plotted in Fig. 5(b). The intensities of 280 and 790 cm^{-1} phonon modes have positive relationship with ordered and disordered domains, respectively. Therefore, an abrupt jump observed at T_C indicates the vanishing of the long range order. There is a striking similarity between the ratio $I_{280\ cm^{-1}}/I_{790\ cm^{-1}}$ and $I_{510\ cm^{-1}}/I_{600\ cm^{-1}}$, both of which change abruptly at $T_C \sim 460$ K, $T_{R-T} \sim 390$ K, and $T_{(R+M+O)-R} \sim 325$ K, as shown in Figs. 5(b) and 5(c), respectively.

For the PIN-PMN-33PT crystal, the most noticeable result of the present study can be derived from an obvious change of Raman spectra around 200 K in the VV and VH geometry in Figs. 1(c), 1(f), 1(i), 4(e), and 4(f). Actually, there is a dip for the intensity of the modes at 600 cm^{-1} and 790 cm^{-1}, as shown in Fig. 6. These high frequency modes from 500 to 800 cm^{-1} are classified as B-O-B stretching according to the mode assignment of PMN and lattice dynamics calculations. The intermediate frequency from 150 to 500 cm^{-1} is attributed to the mixture of B-O-B bending and O-B-O stretching, with the low frequency region below 150 cm^{-1} to the Pb-BO_6 stretching modes.[35] The existence of 790 cm^{-1} mode, originating from first-order Raman scattering related to cubic Raman-active nondegenerate, reveals a double-perovskite structure of Pb-based relaxors.[13,30] It is symmetrically allowed only in a double-perovskite structure, which means that such mode never exists in a single-perovskite structure no matter the structure is cubic or ferroically distorted. Such double-perovskite structure is stable and it cannot be disturbed by a moderate addition of PT to PZN or PMN.[36–38] It shows that there are low-temperature anomalous structures with an onset of antiferrodistortive octahedral rotations by analogy of PZT and tilting angle of

polarization. The *Cm* space group of PZT changes to the *Cc* space group due to an antiferrodistortive phase transition at low temperatures.[39,40] In FE perovskites, the octahedra tilts are not associated with the softening of the Γ_{15} zone-center mode, and do not essentially affect the ferroelectric properties due to the independence of the cation displacements.[41] The relative intensity between $I_{510\,cm^{-1}}$ and $I_{600\,cm^{-1}}$ is changed in the first-order phase transitions at T_C, T_{R-T} and $T_{(R+M+O)-R}$, while it is unchanged below 300 K. It indicates that the low-temperature anomalous structure of the PIN-PMN-33PT is not a simply first-order phase transition. Note that the relative Raman intensities of $I_{510\,cm^{-1}}$ and $I_{600\,cm^{-1}}$ change from $I_{510\,cm^{-1}} > I_{600\,cm^{-1}}$ [in C and R phases, Fig. 5(c)] to $I_{510\,cm^{-1}} < I_{600\,cm^{-1}}$ (in T and coexistence of $R + M_C + O$ phases) at a first-order phase transition. This can be further proven by more obvious change ratio of $I_{510\,cm^{-1}}/I_{600\,cm^{-1}}$ as well as $I_{280\,cm^{-1}}/I_{790\,cm^{-1}}$ at $T_{R-T} \sim 390$ K and $T_C \sim 460$ K than that at $T_{(R+M+O)-R} \sim 325$ K.

Lack of studies on low-temperature phase transformations in ternary systems adds the difficulty to distinguish the structures below room temperature. It is useful to compare the structural phase transitions in other perovskite ferroelectrics with those in the present system because they belong to ABO_3-type and probably have the similar response behaviors.[13,42] In PZT system, low-temperature phase transitions are found in both sides of the MPB region. A high-temperature rhombohedral (*R*3 *m*) phase transforms into a low-temperature rhombohedral (*R*3 *c*) phase at 200 K. Moreover, the space groups for the high-temperature monoclinic and tetragonal phases are *Cm* and *P*4 *mm*, while those for the low-temperature ones are *Cc* and *I*4 *cm* below 200 K, respectively.[23,42] Obviously, the low-temperature anomalous

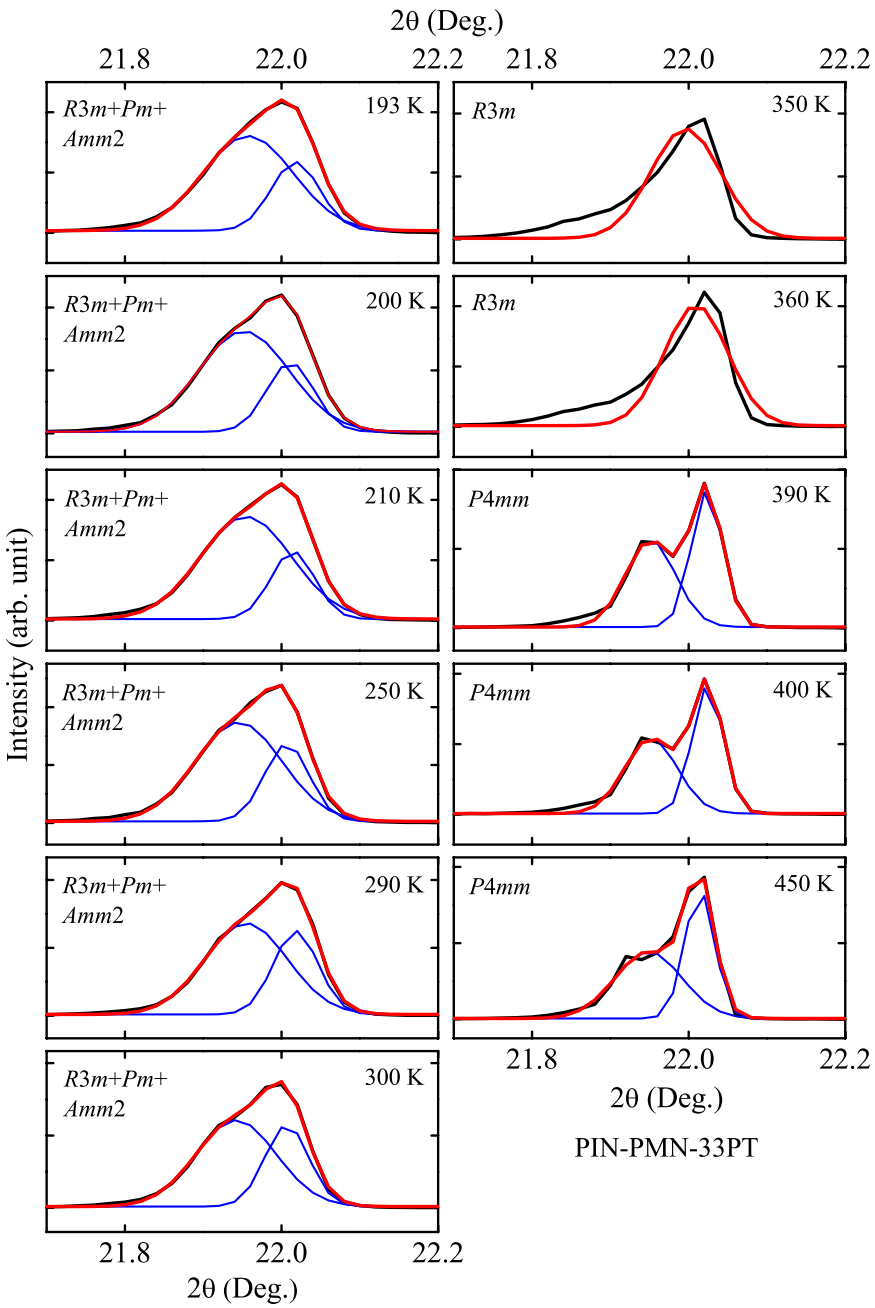

FIG. 7. The (100) diffraction patterns of the PIN-PMN-33PT crystal with the temperature from 193 to 450 K. In order to extract the peak position, the diffraction patterns have been fitted by the Gaussian lineshape analysis.

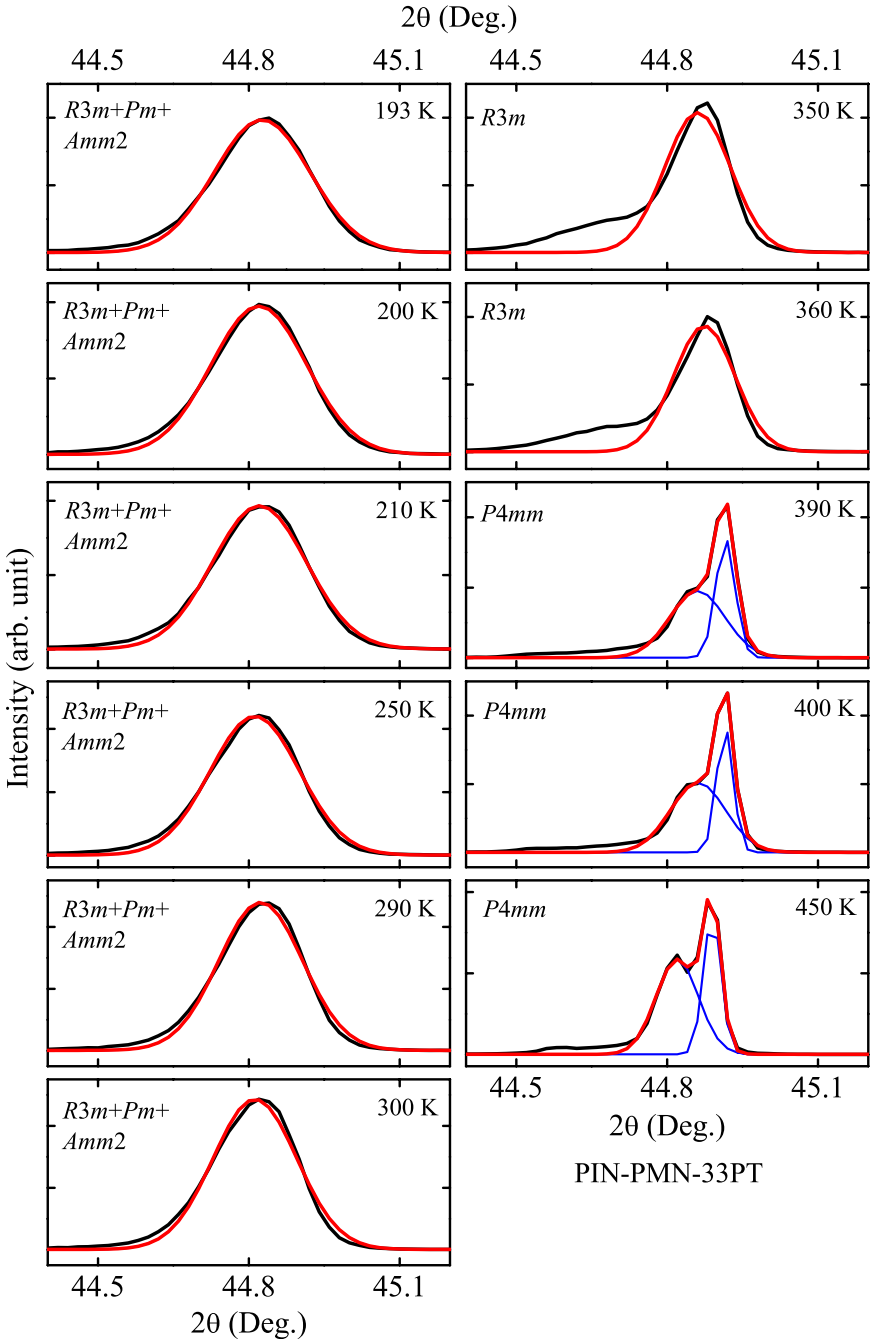

FIG. 8. The (200) diffraction patterns of the PIN-PMN-33PT crystal with the temperature from 193 to 450 K. In order to extract the peak position, the diffraction patterns have been fitted by the Gaussian lineshape analysis.

structure of PIN-PMN-PT is not the case since the *R*3*c*, *Cc*, and *I*4 *cm* phases have been never found in PMN-PT/PIN-PMN-PT systems until now. In PMN-PT solid solutions, the cubic to rhombohedral phase transition of PMN-0.09PT far away from the MPB region is at 283 K, while the rhombohedral to monoclinic phase transition of PMN-0.28PT in the PT poor region near the MPB region is at 273 K.[13] Both of them are the first-order phase transition, which cannot explain the present low-temperature anomalous structures of PIN-PMN-PT due to the contradiction of the unchanged relative intensity of $I_{510\,cm^{-1}}$ and $I_{600\,cm^{-1}}$. For PMN-35PT and PMN-38PT in the PT rich region of the MPB region, the coexistence of T + M_C, or even T + M_C + O below room temperature was found in the PMN-PT system.[9,13] Moreover, upon heating the volume fraction of T phase increases with decreasing phase coexistence of M_C + O. However, the coexistence phases of R + M_C or R + O in the PT poor region of the MPB are considered as thermal stability. The volume fractions of the R and M_C phases can be estimated to 30% and 70% for PMN-0.31PT at 300 K and 20 K, respectively.[9] Hence, the obvious low-temperature anomalous structures cannot be interpreted by coexistence of thermal stable R + M_C or R + O phases.

D. Theoretical explanation and phase diagram

According to the eighth-order Devonshire theory, a phase transition cannot occur directly in the coexistence of R + M_C, no matter whether it is the first-order or second-order. However, the first-order phase transition can occur in the

coexistence of R + O phases.[18] The changes of volume fraction in the R, M_C, and O phases with increasing the temperature are not monotonous, as can be seen from the obvious Raman intensity decreasing from 80 K to 200 K and increasing from 200 K to 300 K in Figs. 1(c), 1(f), 1(i), 4(e), and 4(f). Both peculiarly positive but monotonous band gap narrowing coefficient and negative one are reported, which indicates that there is at least coexistence of two phases in the MPB region.[16] Therefore, we designate the anomalous structures around 200 K as a second-order phase transition from orthorhombic to monoclinic, coexisting with a rhombohedral phase, which are consistent with abnormal optical properties explained by a multiple phase coexistence model.[16,43] Moreover, a phase transition between the rhombohedral and monoclinic phases via orthorhombic one is considered. This means that the volume fractions of all the three coexistent phases change during the phase transitions, including a second-order phase transition between M_C and O phases, and a first-order one between O and R phases. The first-order phase transition between O and R phases coexisting with the M_C phase is different from another two processes at $T_C \sim 460$ K and $T_{R_T} \sim 390$ K, which change from a paraelectric phase to ferroelectric phase or one ferroelectric phase to the other ferroelectric phase without multiple phase structures.

The phenomena can be also confirmed by variable-temperature XRD patterns, as shown in Figs. 7 and 8 for the PIN-PMN-33PT sample. The diffraction patterns are fitted by the Gaussian lineshape analysis to extract the peak positions. The peak locations at different temperature are listed in Table II. It can be seen that the PIN-PMN-PT single crystals are pure perovskite phase. The structure is tetragonal with *P*4 *mm* space group at 390 K. This is evident from Figs. 7 and 8 and Table II, as the (100)/(200) profiles are seen to be doublet. In the tetragonal phase, the XRD profiles of (200) reflections are split into two peaks, the T(200)/(020) and T(002) profiles, whereas it shows only a single peak R (200) in the rhombohedral symmetry because all the planes of (200) are the same lattice parameters.[44–46] Above 390 K, the tetragonal structure can be clearly identified by two distinct peaks for the $(200)_{cub}$ reflection, while the rhombohedral peak disappears. In the tetragonal phase, the area ratio of the splitting right peak over left peak is 1.6:1, which arises from the intensity ratio of the T(200)/(002) $(2\theta_2)$ reflections over the T(002) $(2\theta_1)$ reflection. It confirms that the phase transition from the rhombohedral to tetragonal phase takes place at 390 K, corresponding to the above Raman analysis. With decreasing the temperature, the two peaks of the (100)/(200) diffraction become closer and form a single peak characteristic of the rhombohedral phase at 350 K and 360 K. As the temperature is further decreased down to 300 K, the (100) peak of the rhombohedral phase is replaced by a broadening peak, with the disappearance of the peak $(2\theta_2 = 22.007°)$. It suggests that the rhombohedral phase has been transformed to the coexistence of phases. Note that the similar variations of volume fractions for three coexistence phases T + M_C + O have been observed by synchrotron X-ray powder diffraction measurements in PMN-0.35PT ceramic.[9] Therefore, the coexistence of the orthorhombic, monoclinic, and rhombohedral phases and complex phase behavior are believed to be an intrinsic feature of the PIN-PMN-PT systems.

TABLE II. The position of (100) and (200) diffraction peaks for the PIN-PMN-PT crystals at different temperatures.

Temperature(K)	(100) Peak position 1 $2\theta_1(°)$	(100) Peak position 2 $2\theta_2(°)$	(200) Peak position 1 $2\theta_1(°)$	(200) Peak position 2 $2\theta_2(°)$
193	21.957	22.018	44.826	…
200	21.952	22.011	44.820	…
210	21.955	22.014	44.821	…
250	21.945	22.007	44.812	…
290	21.955	22.018	44.823	…
300	21.942	22.007	44.812	…
350	21.996	…	44.861	…
360	22.010	…	44.874	…
390	21.951	22.023	44.860	44.916
400	21.952	22.024	44.861	44.914
450	21.949	22.014	44.820	44.890

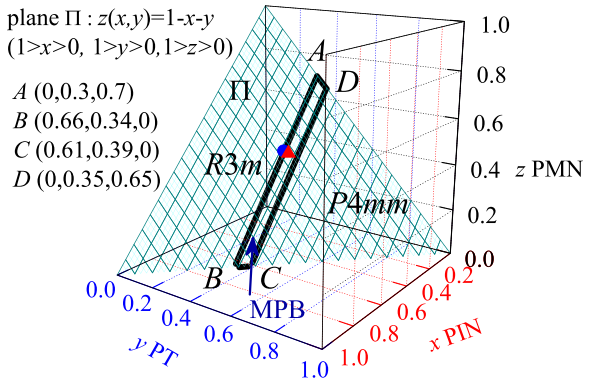

FIG. 9. Phase diagram of the PIN-PMN-PT ternary system at room temperature. Triangle: PIN-PMN-33PT. Circle: PIN-PMN-31PT.

Moreover, Fig. 9 represents a room temperature phase diagram of the *x*PIN-$(1-x-y)$PMN-*y*PT ternary system in a three-dimensional Cartesian coordinate system with the right hand rule. Correspondingly, the relation of *x*PIN, *y*PT, and *z*PMN contents can be described as the plane $\Pi: z = 1 - x - y, (0 < x < 1, 0 < y < 1, 0 < z < 1)$. The dots $A\,(0, 0.3, 0.7)$ and $B\,(0.66, 0.34, 0)$ are the rhombohedral sides of the MPB region in the PMN-PT and PIN-PT systems, while $C\,(0.61, 0.39, 0)$ and $D\,(0, 0.35, 0.65)$ are the tetragonal sides, respectively.[9,47] The triangle and circle dots represent the PIN-PMN-33PT and PIN-PMN-31PT systems, respectively. Other results from XRD experiments also indicated that the MPB region of PIN-PMN-PT is located around PT ~0.33-0.36.[47,48] Combining with these data, it was found that the MPB region of the PIN-PMN-PT crystal can be defined by four lines l_{AB}, l_{BC}, l_{CD}, and l_{DA}, where $l_{AB}: \frac{x}{-0.66} = \frac{y-0.3}{-0.04} = \frac{z-0.7}{0.7}$, $l_{BC}: \frac{x-0.66}{0.05} = \frac{y-0.34}{-0.05}, z = 0$, $l_{CD}: \frac{x-0.61}{0.61} = \frac{y-0.39}{0.04} = \frac{z}{-0.65}$, $l_{DA}: \frac{y-0.35}{0.05} = \frac{z-0.65}{-0.05}, x = 0$. One can safely conclude that the PIN-PMN-PT system also presents the distinct MPB region, which is strongly related to that of the PMN-PT/PIN-PT system.

IV. CONCLUSION

To summarize, the temperature evolution of phonon anomalies for ferroelectric 27PIN-40PMN-33PT and 28PIN-41PMN-31PT crystals reveals new low-temperature anomalous structures. This is due to a first-order phase transition between rhombohedral and orthorhombic phases as well as a second-order one from monoclinic (M_C) to orthorhombic phase occurring at low temperature. It connects with antiphase tilts of oxygen octahedra in analogy with the observations of PZT system reported. Moreover, the relative ratio between $I_{510\,cm^{-1}}$ [E(TO4) mode in rhombohedral phase] and $I_{600\,cm^{-1}}$ [A_1(TO3) mode in rhombohedral phase] in the VH geometry can be an obvious feature of the phase transitions for the Pb-based relaxor ferroelectric systems. Correspondingly, another two structural transitions are observed upon heating. One is the cubic to tetragonal phase transition at 460 K and the other is the tetragonal to rhombohedral at 390 K. In addition, depicting phase diagram of the PIN-PMN-PT crystal in three-dimensional Cartesian coordinate system is a universal method to describe ternary materials. The present study extends understanding of the coexistence of multiple phase symmetries in the PIN-PMN-PT system near the MPB region.

ACKNOWLEDGMENTS

One of the authors (J. J. Zhu) would like to thank Dr. Sohini Kar-Narayan from University of Cambridge for the fruitful discussions and Dr. Yuanyuan Zhang for the XRD experiments. This work was financially supported by Major State Basic Research Development Program of China (Grant Nos. 2011CB922200 and 2013CB922300), Natural Science Foundation of China (Grant Nos. 11374097, 61376129, and 11074076), Projects of Science and Technology Commission of Shanghai Municipality (Grant Nos. 13JC1402100, 13JC1404200, and 11520701300), and the Program for Professor of Special Appointment (Eastern Scholar) at Shanghai Institutions of Higher Learning.

[1]Z. G. Ye, MRS Bull. **34**, 277 (2009).
[2]S. E. Park and T. R. Shrout, J. Appl. Phys. **82**, 1804 (1997).
[3]M. Ahart, M. Somayazulu, R. E. Cohen, P. Ganesh, P. Dera, H. K. Mao, R. J. Hemley, Y. Ren, P. Liermann, and Z. G. Wu, Nature **451**, 545 (2008).
[4]H. Fu and R. E. Cohen, Nature **403**, 281 (2000).
[5]B. Noheda, D. E. Cox, G. Shirane, S. E. Park, L. E. Cross, and Z. Zhong, Phys. Rev. Lett. **86**, 3891 (2001).
[6]R. Guo, L. E. Cross, S.-E. Park, B. Noheda, D. E. Cox, and G. Shirane, Phys. Rev. Lett. **84**, 5423 (2000).
[7]G. S. Xu, K. Chen, D. F. Yang, and J. B. Li, Appl. Phys. Lett. **90**, 032901 (2007).
[8]P. Finkel, H. Robinson, J. Stace, and A. Amin, Appl. Phys. Lett. **97**, 122903 (2010).
[9]B. Noheda, D. E. Cox, G. Shirane, J. Gao, and Z. G. Ye, Phys. Rev. B **66**, 054104 (2002).
[10]F. Li, S. J. Zhang, Z. Xu, X. Y. Wei, J. Luo, and T. R. Shrout, Appl. Phys. Lett. **97**, 252903 (2010).
[11]V. A. Shuvaeva, A. M. Glazer, and D. Zekria, J. Phys.: Condens. Matter **17**, 5709 (2005).
[12]A. K. Singh, D. Pandey, and O. Zaharko, Phys. Rev. B **74**, 024101 (2006).
[13]A. Slodczyk, P. Daniel, and A. Kania, Phys. Rev. B **77**, 184114 (2008).
[14]G. Xu, Z. Zhong, Y. Bing, Z. G. Ye, and G. Shirane, Nature Mater. **5**, 134 (2006).
[15]Z. H. Duan, Z. G. Hu, K. Jiang, Y. W. Li, G. S. Wang, X. L. Dong, and J. H. Chu, Appl. Phys. Lett. **102**, 151908 (2013).
[16]J. J. Zhu, W. W. Li, G. S. Xu, K. Jiang, Z. G. Hu, and J. H. Chu, Acta Mater. **59**, 6684 (2011).
[17]X. L. Zhang, Z. G. Hu, G. S. Xu, J. J. Zhu, Y. W. Li, Z. Q. Zhu, and J. H. Chu, Appl. Phys. Lett. **103**, 051902 (2013).
[18]D. Vanderbilt and M. H. Cohen, Phys. Rev. B **63**, 094108 (2001).
[19]Y. Y. Liao, Y. W. Li, Z. G. Hu, and J. H. Chu, Appl. Phys. Lett. **100**, 071905 (2012).
[20]X. Chen, Z. G. Hu, Z. H. Duan, X. F. Chen, G. S. Wang, X. L. Dong, and J. H. Chu, J. Appl. Phys. **114**, 043507 (2013).
[21]O. Svitelskiy, J. Toulouse, G. Yong, and Z. G. Ye, Phys. Rev. B **68**, 104107 (2003).
[22]J. Frantti, V. Lantto, and J. Lappalainen, J. Appl. Phys. **79**, 1067 (1996).
[23]M. Deluca, H. Fukumura, N. Tonari, C. Capiani, N. Hasuike, K. Kisoda, C. Galassi, and H. Harima, J. Raman Spectrosc. **42**, 488 (2011).
[24]H. Katzke, M. Dietze, A. Lahmar, M. E. Souni, N. Neumann, and S. G. Lee, Phys. Rev. B **83**, 174115 (2011).
[25]E. Husson, L. Abello, and A. Morell, Mater. Res. Bull. **25**, 539 (1990).
[26]J. A. Lima, W. Paraguassu, P. T. C. Freire, A. G. S. Filho, C. W. A. Paschoal, J. M. Filho, A. L. Zanin, M. H. Lente, D. Garcia, and J. A. Eiras, J. Raman Spectrosc. **40**, 1144 (2009).
[27]J. D. Freire and R. S. Katiyar, Phys. Rev. B **37**, 2074 (1988).
[28]N. Waeselmann, B. Mihailova, B. J. Maier, C. Paulmann, M. Gospodinov, V. Marinova, and U. Bismayer, Phys. Rev. B **83**, 214104 (2011).
[29]Y. Yang, Y. L. Liu, L. Y. Zhang, K. Zhu, S. Y. Ma, G. G. Siu, Z. K. Xu, and H. S. Luo, J. Raman Spectrosc. **41**, 1735 (2010).
[30]B. Mihailova, U. Bismayer, B. Guttler, M. Gospodinov, and L. Konstantinov, J. Phys.: Condens. Matter **14**, 1091 (2002).
[31]B. Mihailova, M. Gospodinov, B. Guttler, R. Stosch, and U. Bismayer, J. Phys.: Condens. Matter **19**, 275205 (2007).
[32]B. Mihailova, M. Gospodinov, B. Guttler, R. Stosch, D. Petrova, and U. Bismayer, J. Phys.: Condens. Matter **19**, 246220 (2007).
[33]A.-M. Welsch, B. Mihailova, M. Gospodinov, R. Stosch, B. Guttler, and U. Bismayer, J. Phys.: Condens. Matter **21**, 235901 (2009).
[34]M. El Marssi, R. Farhi, and Yu. I. Yuzyuk, J. Phys.: Condens. Matter **10**, 9161 (1998).
[35]S. A. Prosandeev, E. Cockayne, P. B. Burton, S. Kamba, J. Petzelt, Yu. Yuzyuk, R. S. Katiyar, and S. B. Bakhrushev, Phys. Rev. B **70**, 134110 (2004).
[36]O. Svitelskiy, D. La-Orauttapong, J. Toulouse, W. Chen, and Z. G. Ye, Phys. Rev. B **72**, 172106 (2005).
[37]M. Iwata, Y. Hasegawa, R. Aoyagi, M. Maeda, N. Wakiya, H. Suzuki, and Y. Ishibashi, Ferroelectric **378**, 84 (2009).
[38]J. Cheng, Y. Yand, Y. H. Tong, S. B. Lu, J. Y. Sun, K. Zhu, Y. L. Liu, G. G. Siu, and Z. K. Xu, J. Appl. Phys. **105**, 053519 (2009).
[39]Ragini, S. K. Mishra, D. Pandey, H. Lemmens, and G. V. Tendeloo, Phys. Rev. B **64**, 054101 (2001).
[40]D. M. Hatch, H. T. Stokes, R. Ranjan, Ragini, S. K. Mishra, D. Pandey, and B. J. Kennedy, Phys. Rev. B **65**, 212101 (2002).
[41]B. Noheda, L. Wu, and Y. Zhu, Phys. Rev. B **66**, 060103(R) (2002).
[42]F. Cordero, F. Craciun, and C. Galassi, Phys. Rev. Lett. **98**, 255701 (2007).
[43]J. J. Zhu, W. W. Li, G. S. Xu, K. Jiang, Z. G. Hu, M. Zhu, and J. H. Chu, Appl. Phys. Lett. **98**, 091913 (2011).
[44]C. He, X. Z. Li, Z. J. Wang, X. F. Long, S. Y. Mao, and Z. G. Ye, Chem. Mater. **22**, 5588 (2010).
[45]Z. Xia and Q. Li, Solid State Commun. **142**, 323 (2007).
[46]L. Wang, Q. Li, L. H. Xue, and X. M. Liang, J. Mater. Sci. **42**, 7397 (2007).
[47]C. Augier, M. PhamThi, H. Dammak, and P. Gaucher, J. Eur. Ceram. Soc. **25**, 2429 (2005).
[48]D. W. Wang, M. S. Cao, and S. J. Zhang, J. Eur. Ceram. Soc. **32**, 433 (2012).